Hidden allies: Decoding the core endohyphal bacteriome of *Aspergillus fumigatus*

Daryna Piontkivska[a], João M.P. Jorge[a#], Dalila Mil-Homens[b,c#], Tiago M. Martins[a#], Pedro Crespo[a], Dinah Carvalho[e], José Melo-Cristino[e], Raquel Sá-Leão[a], Gustavo H. Goldman[a,f,g], Cristina Silva Pereira[a]*

[a]Instituto de Tecnologia Química e Biológica António Xavier, Universidade Nova de Lisboa (ITQB NOVA), Oeiras, Portugal
[b]Institute for Bioengineering and Biosciences (iBB) and Institute for Health and Bioeconomy (i4HB), Instituto Superior Técnico, University of Lisbon, Lisboa, Portugal
[c]Department of Bioengineering, Instituto Superior Técnico, University of Lisbon, Lisboa, Portugal
[e]Laboratory of Microbiology, Unidade Local de Saúde Santa Maria, Lisboa, Portugal
[f]Faculdade de Ciências Farmacêuticas de Ribeirão Preto, Universidade de São Paulo, Brazil
[g]National Institute of Science and Technology in Human Pathogenic Fungi, Brazil
[#]equal contributing authors
*corresponding author: Cristina Silva Pereira (spereira@itqb.unl.pt)

Additional File 1: Supplementary Information (MS Word), containing more detailed tables and figures that support the main figures panels at the main text:

Fig. S1. Bacteria found in negative controls amplification and extraction.

Fig. S2. A, Veen diagram displaying ASVs overlaps found in B, Pearson's correlation coefficients between fungal bacteriome at genus level before and after antibiotic pressure.

Fig. S3. Maximum likelihood midpoint rooted tree of the 100 most abundant bacterial ASVs across the sample set.

Fig. S4. A, Minimum spanning network of *Aspergillus fumigatus* isolates genotyped at nine microsatellite loci; B, Discriminant analysis of principal components and C, its density plot.

Table S1. Minimal inhibitory concentrations of each tested antifungal drug against each *Aspergillus fumigatus* strains.

Fig. S5. Infection capacity of each *A. fumigatus* clinical isolate and one soil isolate (Af_SI.00) using *Galleria mellonella* as infection model.

Table S2. Ratio and derived percentages of 18S/16S rDNA in spores.

Fig. S6. Stacked bar chart showing the relative abundance ASVs from the bacterial V3-V4 hypervariable region of 16S rRNA sequences, taxonomically classified at genus level.

Fig. S7. Phylogenetic tree of the core bacteriome.

Fig. S8. Prediction of the ecologically relevant functions of the *Aspergillus fumigatus* isolates bacteriome.

Fig. S9. Metagenome analysis of whole genome sequencing reads from two clinical isolates.

Fig. S10. (A) Shannon diversity, richness, and evenness of the fungal bacteriome in different infection capacity groups; (B) Hierarchical clustering heat map of fungal bacteriome using Bray-Curtis distance, without core bacteriome.

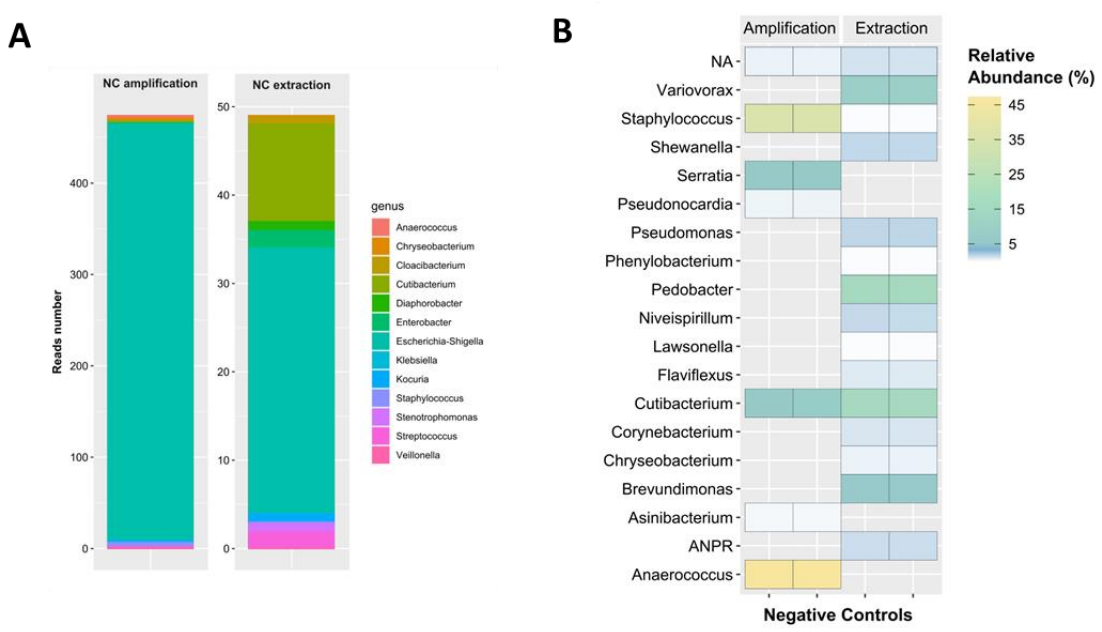

Fig. S1. (A) Bacteria found in negative controls amplification and extraction. All bacterial genera identified in negative control samples were excluded from further analysis (B) Genus-level profile of contaminant ASVs found in negative controls of PCR amplification and DNA extraction, performed in 2 separate days. All bacterial ASVs present in negative control samples were excluded from further analysis. ANPR stands *for Allorhizobium-Neorhizobium-Pararhizobium-Rhizobium* group.

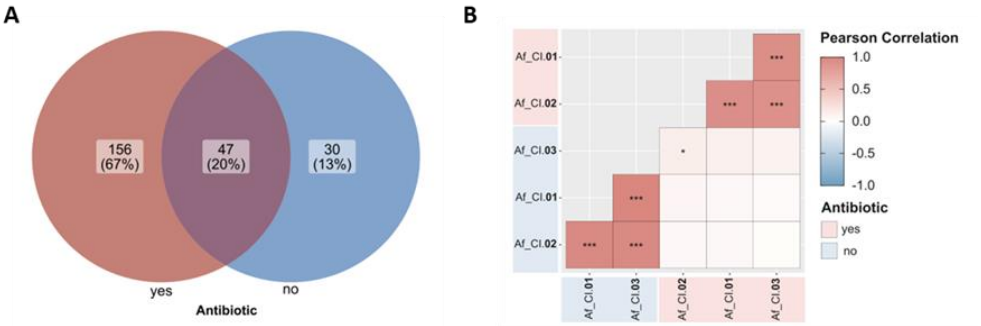

Fig. S2. (A) Veen diagram displaying ASVs overlaps found in (B) Pearson's correlation coefficients between fungal bacteriome at genus level before (no) and after (yes) antibiotic pressure. Note that the 47 common ASVs were found at relative high abundances in mycelia cultivated in media both without and with antibiotic selection, representing 70-78% and 69-75% of the total relative abundance, respectively. Asterisks indicate significant correlations *P ≤ 0.01; ***P ≤ 0.0001.

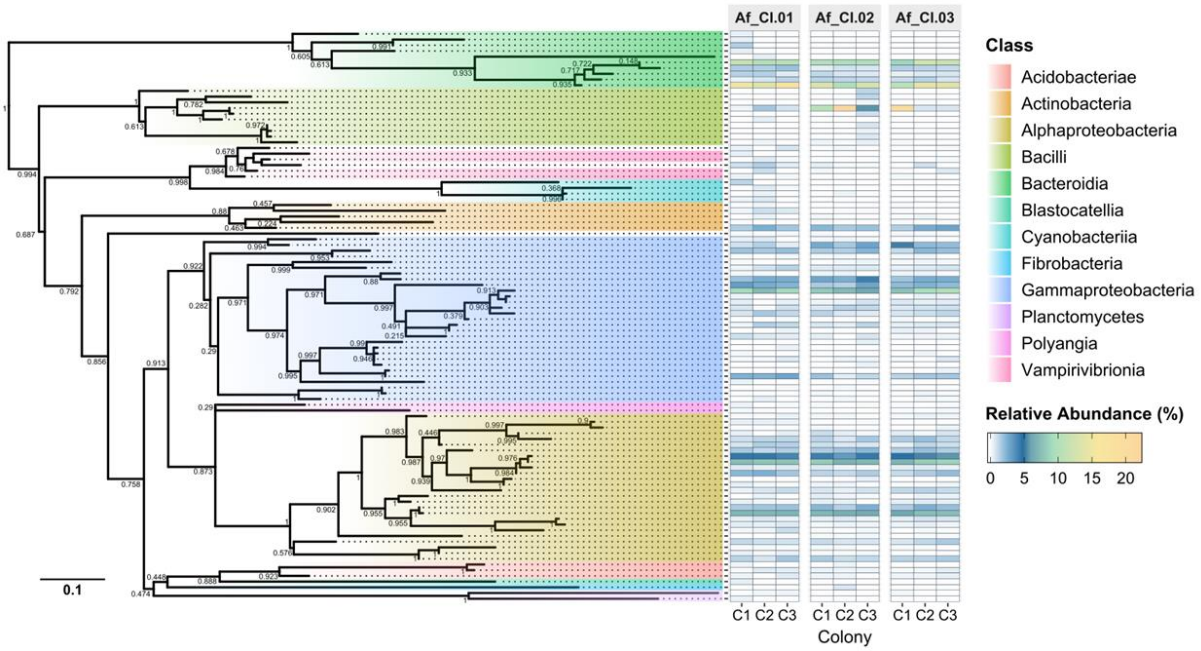

Fig. S3. Maximum likelihood midpoint rooted tree of the 100 most abundant bacterial ASVs across the sample set (corresponding to ~95% of total relative abundance in each sample). The phylogenetic tree was constructed using the general time reversible model with the rate variation among sites described by a gamma distribution and the proportion of invariable sites (GTR + G + I model). Background colors indicate bacterial ASVs assigned at class level. Tree constriction was based on the region V4 of 16S rRNA gene sequences, applying 1000 bootstrap replications to estimate confidence. Bootstrap values are indicated above or below the branches. The scale bar indicates nucleotide substitutions per site. Heatmap shows the relative abundances of bacterial ASVs found in tested fungal clinical isolates, comparing three single spore colonies (C_1, C_2, C_3). The color intensity shows the ASV percentage in each sample (note that in the color key the dark blue corresponds to 5%).

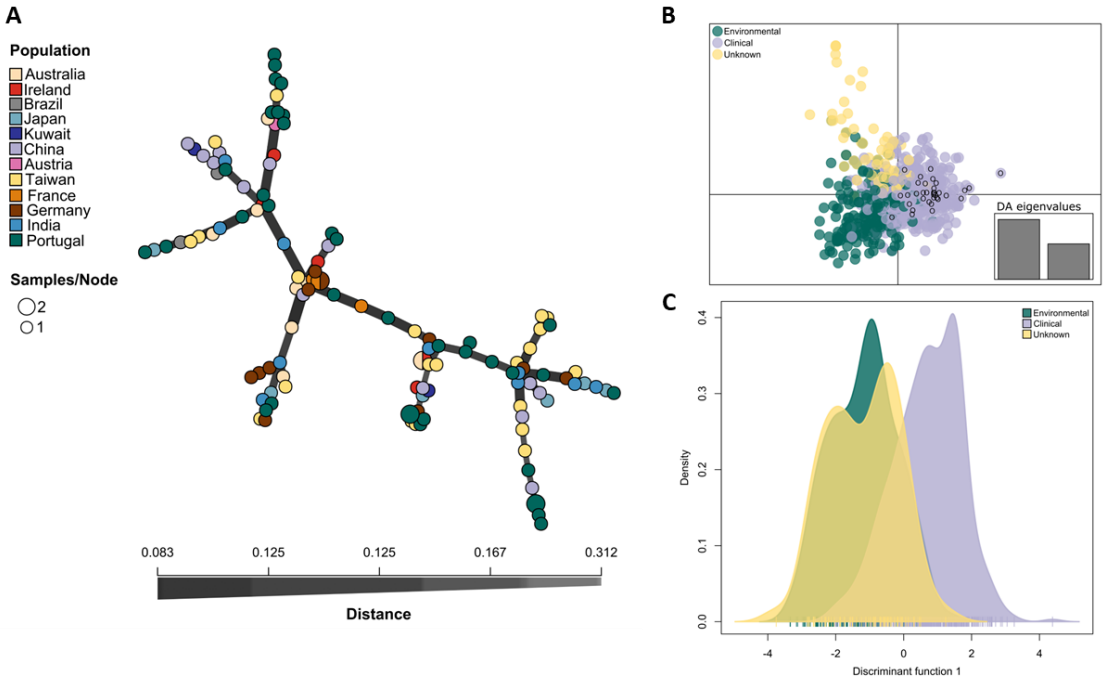

Fig. S4. (A) Minimum spanning network of *Aspergillus fumigatus* isolates genotyped at nine microsatellite loci. The various genotypes of clinical isolates are represented by circles, with colors corresponding to their respective countries. The thickness of the connecting lines signifies the relatedness between the linked isolates, as determined by Bruvo's distance using microsatellite genotyping data. Values approaching zero indicate identical isolates, whereas values nearing one indicate unrelated isolates. (B) Discriminant analysis of principal components (DAPC), clinical strains from Portugal analyzed in this study are indicated with an open black circle above the respective spot in DAPC and are well spread amongst other clinical strains from around the world. (C) Density plot from a modified DAPC, illustrating the characteristics of the first discriminant function.

Table S1. Minimal inhibitory concentrations of each tested antifungal drug against each *Aspergillus fumigatus* strains. The strains were classified as resistant or susceptible according to breakpoint table v 10.0, 2020[#] defined by European Committee on Antimicrobial Susceptibility Testing (EUCAST).

	Amphotericin B		Voriconazole		Posaconazole	
Isolate	**MIC ($mg \cdot L^{-1}$)**	**Classification**	**MIC ($mg \cdot L^{-1}$)**	**Classification**	**MIC ($mg \cdot L^{-1}$)**	**Classification**
Af293	1.0	Susceptible	1.0	Susceptible	0.5	Susceptible
Af_SI.00	1.0	Susceptible	1.0	Susceptible	0.5	Susceptible
Af_CI.01	1.0	Susceptible	1.0	Susceptible	0.5	Susceptible
Af_CI.02	1.0	Susceptible	1.0	Susceptible	0.5	Susceptible
Af_CI.03	1.0	Susceptible	2.0	Resistant	1.0	Resistant
Af_CI.06	1.0	Susceptible	1.0	Susceptible	0.5	Susceptible
Af_CI.07	2.0	Resistant	1.0	Susceptible	0.5	Susceptible
Af_CI.08	2.0	Resistant	2.0	Resistant	1.0	Resistant
Af_CI.09	1.0	Susceptible	2.0	Resistant	1.0	Resistant
Af_CI.11	2.0	Resistant	1.0	Susceptible	0.5	Susceptible
Af_CI.12	1.0	Susceptible	1.0	Susceptible	1.0	Resistant
Af_CI.13	1.0	Susceptible	1.0	Susceptible	1.0	Resistant
Af_CI.14	1.0	Susceptible	2.0	Resistant	1.0	Resistant
Af_CI.15	2.0	Resistant	2.0	Resistant	1.0	Resistant
Af_CI.16	1.0	Susceptible	1.0	Susceptible	1.0	Resistant
Af_CI.17	2.0	Resistant	2.0	Resistant	1.0	Resistant
Af_CI.18	1.0	Susceptible	2.0	Resistant	1.0	Resistant
Af_CI.19	2.0	Resistant	2.0	Resistant	0.5	Susceptible
Af_CI.20	1.0	Susceptible	2.0	Resistant	1.0	Resistant
Af_CI.22	2.0	Resistant	1.0	Susceptible	1.0	Resistant
Af_CI.23	2.0	Resistant	1.0	Susceptible	1.0	Resistant
Af_CI.24	2.0	Resistant	1.0	Susceptible	1.0	Resistant
Af_CI.27	2.0	Resistant	1.0	Susceptible	1.0	Resistant
Af_CI.28	1.0	Susceptible	1.0	Susceptible	1.0	Resistant
Af_CI.30	1.0	Susceptible	1.0	Susceptible	1.0	Resistant
Af_CI.31	2.0	Resistant	1.0	Susceptible	1.0	Resistant
Af_CI.32	2.0	Resistant	1.0	Susceptible	1.0	Resistant
Af_CI.34	2.0	Resistant	1.0	Susceptible	1.0	Resistant
Af_CI.36	1.0	Susceptible	1.0	Susceptible	1.0	Resistant
Af_CI.37	2.0	Resistant	1.0	Susceptible	1.0	Resistant
Af_CI.38	2.0	Resistant	2.0	Resistant	0.5	Susceptible
Af_CI.39	2.0	Resistant	1.0	Susceptible	0.5	Susceptible
Af_CI.41	1.0	Susceptible	2.0	Resistant	1.0	Resistant

Af_CI.42	1.0	Susceptible	1.0	Susceptible	0.5	Susceptible
Af_CI.43	2.0	Resistant	2.0	Resistant	0.5	Susceptible
Af_CI.44	1.0	Susceptible	1.0	Susceptible	0.5	Susceptible
Af_CI.45	2.0	Resistant	2.0	Resistant	1.0	Resistant
Af_CI.46	2.0	Resistant	2.0	Resistant	0.5	Susceptible
Af_CI.47	1.0	Susceptible	1.0	Susceptible	1.0	Resistant

[#]Arendrup MC, Friberg N, Mares M, Kahlmeter G, Meletiadis J, Guinea J, Andersen C, Arikan-Akdagli S, Barchiesi F, Chryssanthou E: How to interpret MICs of antifungal compounds according to the revised clinical breakpoints v. 10.0 European committee on antimicrobial susceptibility testing (EUCAST). *Clin Microbiol Infect* 2020, **26**(11):1464-1472.

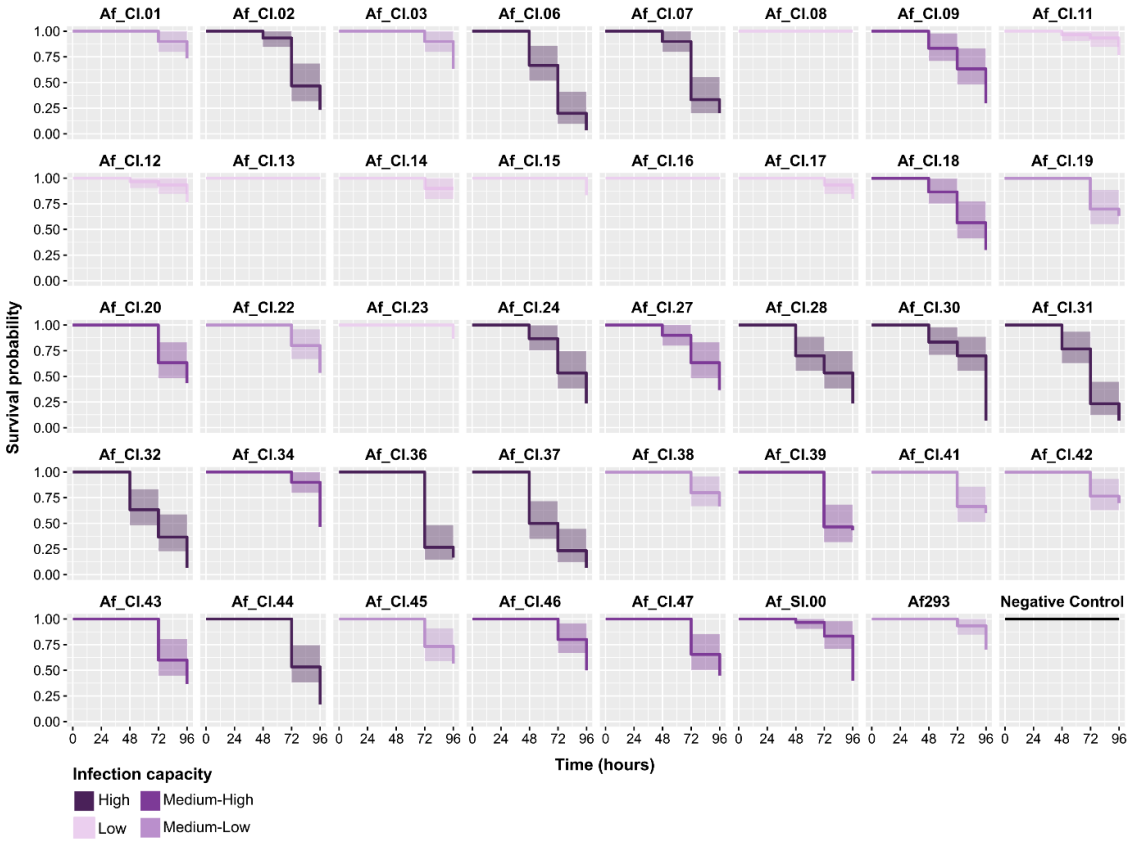

Fig. S5. Infection capacity of each *A. fumigatus* clinical isolate and one soil isolate (Af_SI.00) using *Galleria mellonella* as infection model (n=30). The infection capacity was assessed individually (infection with 10^7 spores per larvae), showed by Kaplan-Meier survival curves discriminating the survival probability over 96h. Negative control corresponds to injection of saline solution.

Table S2. Ratio and derived percentages of 18S/16S rDNA in spores (~10^8 spores·mL^{-1}) and 24-old mycelia of several *A. fumigatus* strains (n=8). $Ratio_{18S/16S} = 2^{(Ct18S\ rDNA - Ct16S\ rDNA)}$ and the18S% = $Ratio_{18S/16S}$ / ($Ratio_{18S/16S}$ + 1) *100 and 16S% = 100 – 18S%[#].

Strain	18S/16S Ratio		Percentages (%)			
	Mycelium	Spores	Mycelium		Spores	
			18S%	16S%	18S%	16S%
Af_SI.00	164.7	73.1	99.4	0.6	98.7	1.4
AF_CI.01	106.9	77.6	99.1	0.9	98.7	1.3
AF_CI.02	91.6	134.8	98.9	1.1	99.3	0.7
AF_CI.03	104.9	108.2	99.1	0.9	99.1	0.9
AF_CI.06	108.4	61.7	99.1	0.9	98.4	1.6
AF_CI.07	216.3	98.6	99.5	0.5	99.0	1.0
AF_CI.08	*n.d.*	228.8	*n.d.*	*n.d.*	99.6	0.4
AF_CI.12	65.5	287.2	98.5	1.5	99.7	0.4
AF_CI.18	181.4	274.3	99.5	0.6	99.6	0.4

n.d., not done; AF.CI.018, after 48-h, formed a scarce mycelium, insufficient to extract DNA. Oligonucleotide pairs were: (i) 16S. CTCCTACGGGAGGCAGCACT (forward) and ATTACCGCGGCTGCTGG (reverse) and (ii) 18S. CGATAACGAACGAGACCT (forward) and AICCATTCAATCGGTAIT (reverse) using RT-qPCR (CFX96 Thermocycler. Bio-Rad). Each 10 µL reaction mixture included 5 µL of SsoFast Evagreen® Supermix (Bio-Rad). 0.5 µL of each primer (10 µM). 3 µL of PCR-quality water and 1 µL of template rDNA at a concentration of 10 ng/µL (96 well plates). The PCR conditions were as follows: enzyme activation at 95 ºC for 120 s; 35 cycles of denaturation at 94 ºC for 20 s. annealing at 64 ºC (16S) or 58 ºC (18S) for 30 s and extension at 68 ºC for 30 s. Melting curves from the RT-qPCR assays were examined to verify primer specificity. All assays were done using three biological replicates, and three to five technical replicates, besides adequate controls.

Ostheim P, Alemu S, Tichý A, Sirak I, Davidkova M, Stastna MM, Kultova G, Schuele S, Paunesku T, Woloschak G: Examining potential confounding factors in gene expression analysis of human saliva and identifying potential housekeeping genes. Sci Rep 2022, 12(1):2312.

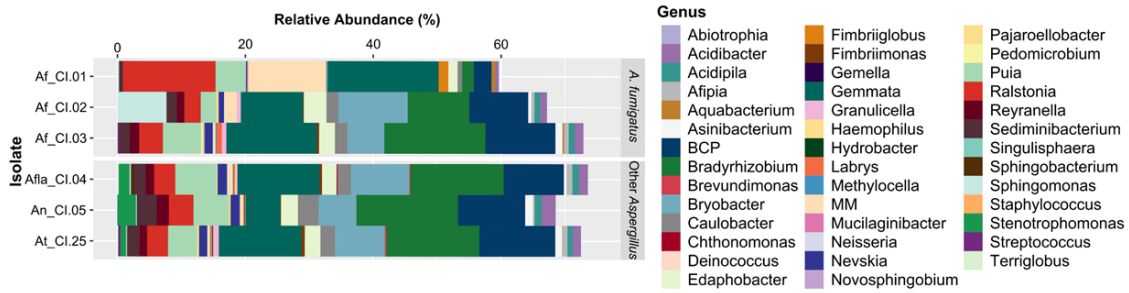

Fig. S6 – Stacked bar chart showing the relative abundance ASVs from the bacterial V3-V4 hypervariable region of 16S rRNA sequences, taxonomically classified at genus level. Showing the comparison between bacteriome found in 3 *A. fumigatus* clinical isolates (same as Fig. 3) with three additional *A. terreus* (At_CI.25), *A. niger* (An_CI.05), and *A. flavus* (Afla_CI.04) clinical isolates. Low abundance taxa were deleted from the visualization. The order of bacterial genus in the legend is according with its position in the chart.

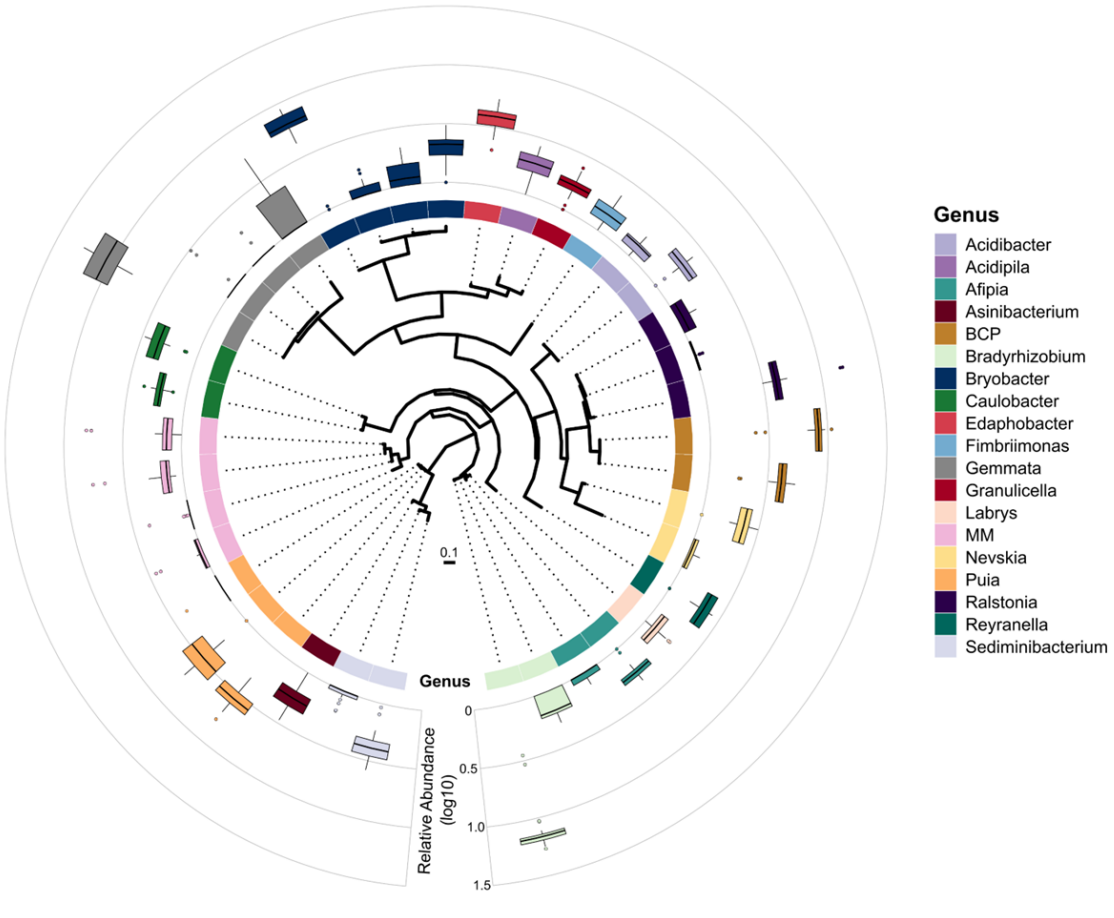

Fig. S7. Phylogenetic tree of the core bacteriome. The scale bar indicates nucleotide substitutions per site. Log_{10} transformed relative abundances.

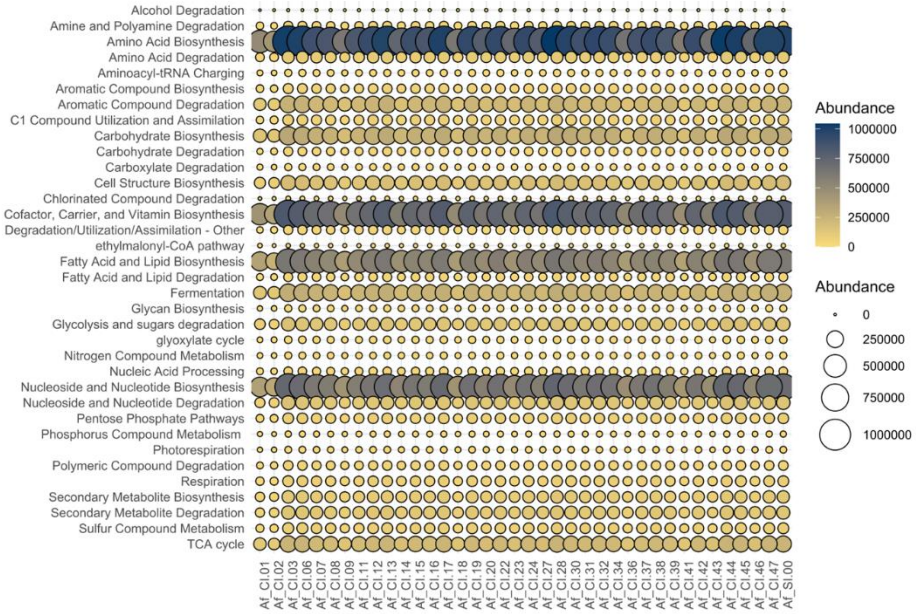

Fig. S8. Prediction of the ecologically relevant functions of the *Aspergillus fumigatus* isolates bacteriome. Picrust2 prediction of the ecological functions of core bacteria (75% prevalence with at least 0.1% detection threshold) using the relative abundance ASVs from the bacterial V3-V4 hypervariable region of 16S rRNA sequences.

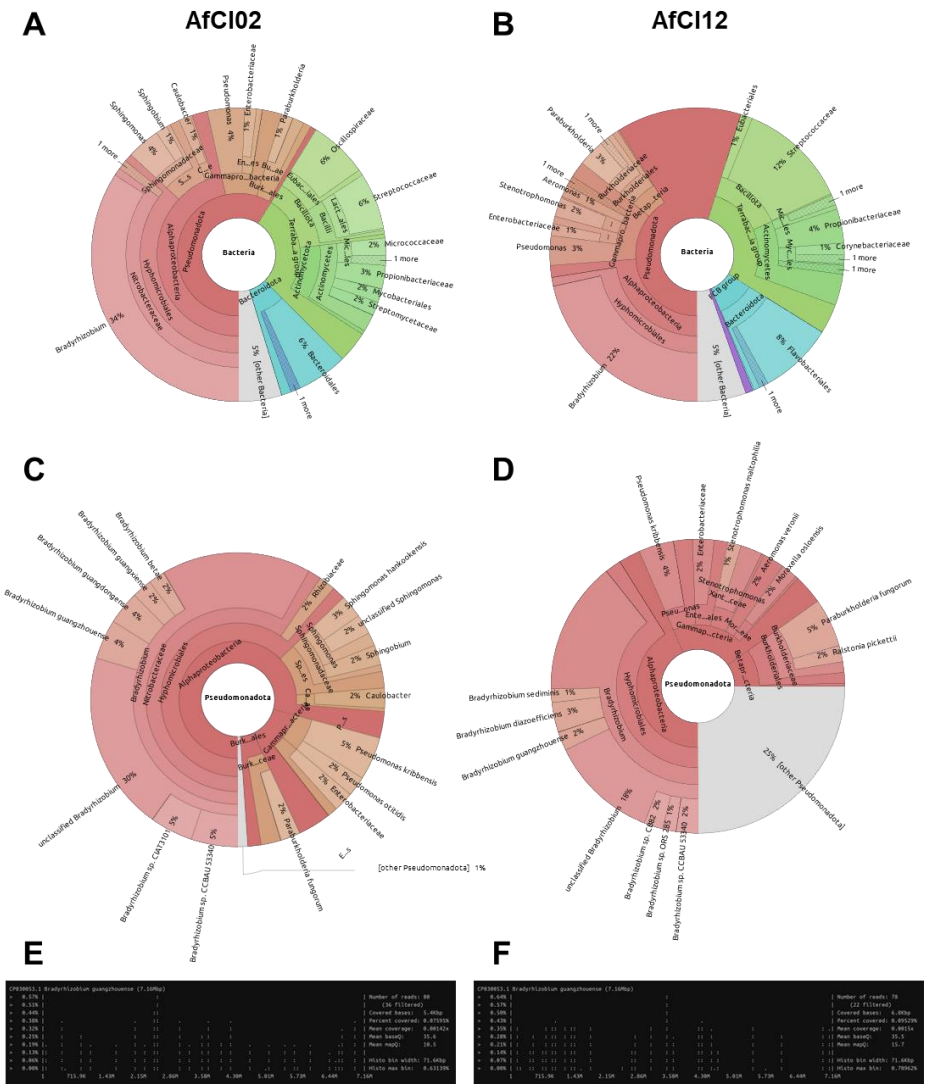

Fig. S9. Metagenome analysis of whole genome sequencing reads from two clinical isolates. Highlight of reads matched to Bacteria (panel A and B; 466 and 619 counts respectively for Af_CI.02 and Af_CI.12), or Pseudomonadota (C and D) using Kraken, and genome coverage of reads aligned to *Bradyrhizobium guangzhouense* CCBAU 51670 (acc. no. CP030053) (E and F).

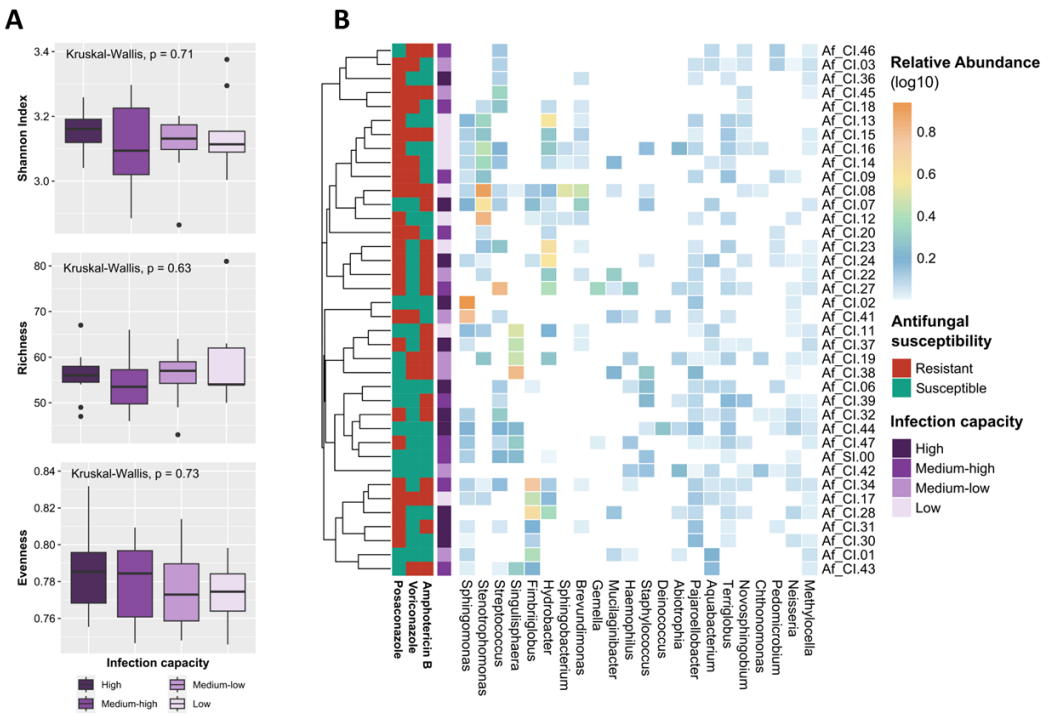

Fig. S10. (A) Shannon diversity, richness, and evenness of the fungal bacteriome in different infection capacity groups. Kruskal-Wallis test was used to test for significant differences between groups. (B) Hierarchical clustering heat map of fungal bacteriome using Bray-Curtis distance, without core bacteriome.